Temperature fluctuations relevant to thermal-plume dynamics in turbulent rotating Rayleigh-Bénard convection

Shan-Shan Ding,[1] Hui-Min Li,[1,2] Wen-Dan Yan,[1] and Jin-Qiang Zhong[1,*]

[1]*Shanghai Key Laboratory of Special Artificial Microstructure Materials and Technology and School of Physics Science and Engineering, Tongji University, Shanghai 200092, China*

[2]*Engineering Practice Center, Tongji University, Shanghai 200092, China*

(Received 12 August 2018; published 4 February 2019)

We present measurements of temperature fluctuations in turbulent rotating Rayleigh-Bénard convection. The temperature variance exhibits power-law dependence on the fluid height outside the thermal boundary layers irrespective of the rotating rates. Rotations increase the magnitudes of temperature variance, but reduce the skewness and kurtosis, leading to Gaussian-like temperature distributions. We derive a general theoretical expression for all statistical moments of temperature in terms of the dynamical properties of the thermal plumes, based on the findings that both the amplitude and time width of thermal plumes are log-normally distributed. Our model replicates the statistical properties of the temperature fluctuations and reveals the physical origin of their rotation dependence. Rotations increase the temperature amplitude of thermal plumes by virtue of the Ekman pumping process, but reduce the variations of the plume amplitude in time, presumably through the suppression of turbulent mixing between the plumes and the ambient fluid.

DOI: 10.1103/PhysRevFluids.4.023501

I. INTRODUCTION

Large temperature fluctuations are a prominent feature of thermally driven turbulence in which one observes local fluid temperatures with large deviations from their mean values [1,2]. The statistical properties of temperature fluctuations, such as their probability distribution functions, the scalings of their power spectra and the corresponding structure functions, and so forth, are fundamental characterizations of turbulent thermal flows [3–8].

In turbulent thermal convection, the large excursions of local fluid temperature are often ascribed to thermal disturbances of coherent flow structures [9–11]. Thermal plumes, one of the primary coherent structures in thermal convection, have been shown to produce pronounced temperature fluctuations as they erupt from the thermal boundary layers (BLs) intermittently. Since thermal plumes carry heat across the convective fluid, their motions and dynamical interactions with the background turbulence play a crucial role in determining the distribution of energy dissipation and local heat transport. In a recently developed theory [12], Grossmann and Lohse treated the role of plumes explicitly, taking into account their contributions to the thermal dissipation as detached thermal boundary layers. Understanding the dynamical and statistical properties of thermal plumes and their influences on the fluid temperature fluctuations is important for further investigations of the flow dynamics and the turbulent transport processes in thermal convection systems.

In many geophysical and astrophysical systems, turbulent convection is strongly influenced by the background rotations [13–15]. In a paradigmatic laboratory model for studying rotationally influenced convection flows in a rotating Rayleigh-Bénard convection (RBC) system, it has been elucidated that the influences of rotational friction and thermal forcing may have a profound effect

*Corresponding author: jinqiang@tongji.edu.cn

on the morphology of the turbulent flow structures [16,17]. For certain parameter regimes, thermal plumes are stretched into columnar vortices through the Ekman pumping process, which extracts efficiently fluid from the thermal BLs, leading to noticeable enhancement of the global heat transport [16–20]. However, there remain the natural questions of how the local fluid temperature responds to the substantial variations of the plume structures under the rotational constraints and whether new information of the coherent flow structures can be extracted and revealed by the statistical properties of temperature fluctuations. Recent experiments report that deliberate rotations change the primary features of the local fluid temperatures in terms of stronger but more symmetrically distributed fluctuations outside the thermal BLs [21–23].

In this paper we present experimental studies of temperature fluctuations and thermal plume dynamics in turbulent rotating RBC. Results of the vertical temperature profiles reveal that the temperature variance σ^2 exhibits a power-law dependence on the fluid height outside the thermal BL, irrespective of the strength of the applied rotations. The background rotations, however, reduce the decreasing rates of σ^2 toward the interior fluid and give rise to greater thermal disturbances. Rotations reduce the high-order statistical moments (skewness and kurtosis), indicating a Gaussian-like temperature distribution. We derive in general a theoretical expression for the statistical moments of temperature fluctuations, based on the experimental findings that both the probability density functions (PDFs) of the plume amplitude and the time width are dictated by log-normal distributions. Our model is shown to be capable of replicating the rotation dependence of the temperature fluctuations. We suggest that, on one hand, rotations enhance the temperature amplitude of the thermal plumes in the mixing zone by virtue of the Ekman pumping process and result in a larger magnitude of temperature variance. On the other hand, rotations provide dynamical constraints to suppress the turbulent mixing of the plumes with the ambient fluid and reduce the variations of the plume amplitude in time, leading to smaller values of skewness and kurtosis and more symmetrical fluid temperature distributions.

II. EXPERIMENTAL SETUP

The experiment was performed in a cylindrical convection sample that had a diameter of $D = 24.00$ cm and a height $L = 24.00$ cm, yielding an aspect ratio 1.00. The Rayleigh number $\mathrm{Ra} = \alpha g \Delta T L^3/\kappa\nu$ covered the range $3.8 \times 10^8 \leqslant \mathrm{Ra} \leqslant 4.3 \times 10^9$ (g is the gravitational acceleration, α is the thermal expansion coefficient, ν is the viscosity, κ is the thermal diffusivity, and ΔT the applied temperature difference). Deionized water at a mean temperature of 20.00 °C was used as the working fluid. The Prandtl number $\mathrm{Pr} = \nu/\kappa = 6.70$ remained constant. Constructions of the convection sample and its auxiliary thermal-protection facilities have been described before [24–26]. The whole apparatus was built on a rotating table. We used rotating rates up to 1.05 rad/s. The inverse Rossby number $1/\mathrm{Ro} = 2\Omega\sqrt{L/\alpha g \Delta T}$ varied in the range $0.0 \leqslant 1/\mathrm{Ro} \leqslant 8.0$, where noticeable enhancement of heat transport was observed [16,25]. Local fluid temperature was measured using a hermetically sealed glass-encapsulated thermistor with a diameter of 0.38 mm and a response time of 30 ms. As shown in the inset of Fig. 1(a), the thermistor was guided to moved along the central line of the sample by a stainless steel capillary mounted on a translational stage. Before the temperature measurements were performed, the thermistor was calibrated in a separate calibration facility with a precision of a few millidegrees Kelvin [24].

III. RESULTS AND DISCUSSION

A. Statistical properties of temperature fluctuations

Figure 1(a) shows a time trace of the fluid temperature $T(t)$ measured outside the thermal BL above the bottom plate for $\mathrm{Ra} = 4.22 \times 10^9$ and $1/\mathrm{Ro} = 0.0$. In this example, one sees clearly that the time series consists of intermittent spikes when $T(t)$ rises abruptly above the background of steady fluctuations. The intensity of fluctuations in $T(t)$, characterized by the temperature variance $\sigma^2 \equiv \langle [T(t) - \langle T \rangle]^2 \rangle$, is depicted as a function of the fluid height z for several values of Ro in

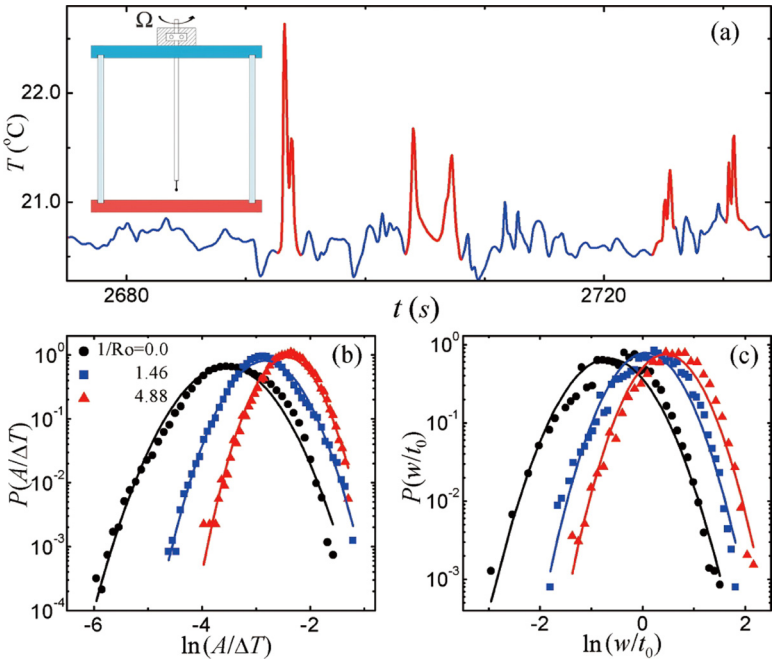

FIG. 1. (a) Time series of the fluid temperature measured at height $z = 24\lambda$ for $\mathrm{Ra} = 4.22 \times 10^9$ and $1/\mathrm{Ro} = 0.0$. The thickness of the thermal BL λ is determined by the position of the maximum temperature variance. Red spikes are recognized as plume signals. The inset shows a schematic of the movable temperature probe mounted in a rotating RBC apparatus. Also shown are PDFs of (b) the normalized plume amplitude $A/\Delta T$ and (c) the plume time width w/t_0. Here $t_0 = \sqrt{L/\alpha g \Delta T}$ is the free-fall time. The solid curves show log-normal distributions.

Fig. 2(a). In the mixing zone outside the thermal BL ($\lambda \leqslant z \leqslant 24\lambda$), our nonrotating data [black circles in Fig. 2(a)] show that with an increasing fluid height $\sigma(z)$ decreases and follows a power function $\sigma(z) = \sigma_0(z/\lambda)^{-\beta}$. These results are consistent with previous experiments [27–29] and a recent theoretical model [29], but disagree with other measurements in which logarithmic profiles of $\sigma(z)$ are observed [30–32]. When rotations are applied such similar behavior is maintained in the profile of $\sigma(z)$, irrespective of the rotating rates.

Fitting power-law functions to the data of $\sigma(z)$ outside the thermal BL, we obtain the decay rates β of $\sigma(z)$ toward the center fluid for all applied rotating rates. Figure 2(b) shows the results of $\beta(1/\mathrm{Ro})$ for various Ra. Starting from the nonrotating value of 0.62, β decreases with increasing rotation rates until it reaches a minimum of 0.23 at $1/\mathrm{Ro} \approx 5.0$ and then approaches asymptotically 0.25 ± 0.02 in the fastest rotating regime of the present study, indicating a greater level of thermal fluctuation resulting from stronger rotations. It can be seen that the data of $\beta(1/\mathrm{Ro})$ for different values of Ra are superimposed on each other on one universal curve, suggesting that the decay rate of $\sigma(z)$ is determined by Ro but independent of Ra. The data of $\sigma(z)/\sigma_0$ inside the thermal BL ($z \leqslant \lambda$) appear to be independent of the applied rotations.

The properties of the thermal fluctuations under deliberate rotations are investigated further through measurements of their high-order statistical moments, the temperature skewness ($\mathrm{Sk} \equiv \langle [T(t) - \langle T \rangle]^3 \rangle / \sigma^3$) and kurtosis ($\mathrm{Ku} \equiv \langle [T(t) - \langle T \rangle]^4 \rangle / \sigma^4$). Figures 3(a) and 3(b) depict profiles of $\mathrm{Sk}(z)$ and $\mathrm{Ku}(z)$ for various rotating rates. Despite the increase of the temperature variance in the mixing zone, the magnitudes of both Sk and Ku decrease under stronger rotations. These findings imply that fluctuations of the fluid temperature are varying more symmetrically in time and the resultant PDFs are closer to a Gaussian distribution. Inside the thermal BLs ($z \leqslant \lambda$), Sk is negative

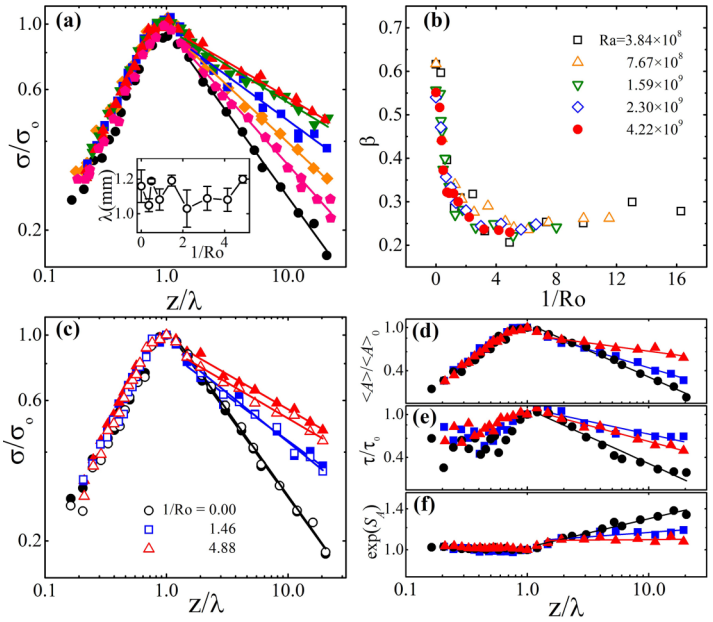

FIG. 2. (a) Normalized temperature standard deviation σ/σ_0 for various 1/Ro. Data are for 1/Ro = 0.0 (black circles), 0.37 (pink hexagons), 0.49 (orange diamonds), 1.46 (blue squares), 3.17 (green down triangles), and 4.88 (red up triangles). The inset shows the thermal boundary layer thickness λ as a function of 1/Ro. The error bars present the standard deviation. (b) Results for the exponent β as a function of 1/Ro for various Ra. (c) Theoretical results (open symbols) of σ/σ_0 compared with the experimental data (closed symbols). (d)–(f) Statistical properties of the thermal plumes: vertical profiles of the (d) plume amplitude $\langle A\rangle/\langle A\rangle_0$, (e) occupation time fraction τ/τ_0, and (f) $\exp(S_A)$. The results in (a), (c), and (d)–(f) are for Ra = 4.22×10^9. Here σ_0, $\langle A\rangle_0$, and τ_0 denote respective values measured at $z = \lambda$. The straight lines are power-law fittings.

with its magnitude dependent on the rotating rates. However, the magnitude of Ku is close to 3.0 and independent of the Rossby number, which reveals a Gaussian-like temperature distribution.

B. Statistical properties of thermal plumes

The power-law profile of temperature fluctuation $\sigma(z)$ in free convection was first proposed under the assumption that heat flux remains a constant along a vertical axis [33]. As the thermal plumes serve as the basic element of heat transport, we suggest that the dynamics properties of the thermal plumes determine the profile of $\sigma(z)$. Here we analyze the temperature signals and consider the contributions to the temperature fluctuations by the plume disturbance and by the background turbulence separately. In our analysis, we identify the thermal plume signals [the red spikes in Fig. 1(a)] from the background turbulence [blue curves in Fig. 1(a)], following a three-step algorithm. A similar approach has been employed in earlier studies of turbulent convection in Ref. [34].

(i) Sections of time series with rapidly varying temperature $T_r(t)$ are identified as plume signals if the rate of temperature variation within $T_r(t)$ satisfies the criterion $dT > \eta\sigma$. Here $dT = [T(t + dt) - T(t)]$ is the temperature increment during the time interval $dt = 1/f$ with the data sampling frequency in the experiment $f = 13$ Hz. In the present work we use a threshold value $\eta = 0.25$.

(ii) The local temperature maximum T_m at the moment $t = t_m$ in the section of $T_r(t)$ is identified as the maximum plume temperature [Fig. 4(a)].

(iii) Two moments t_i and t_e around t_m with $t_i < t_m$ and $t_e > t_m$ when the temperature reaches minima are identified as the initial time and ending time of the plume signal, respectively. Sections

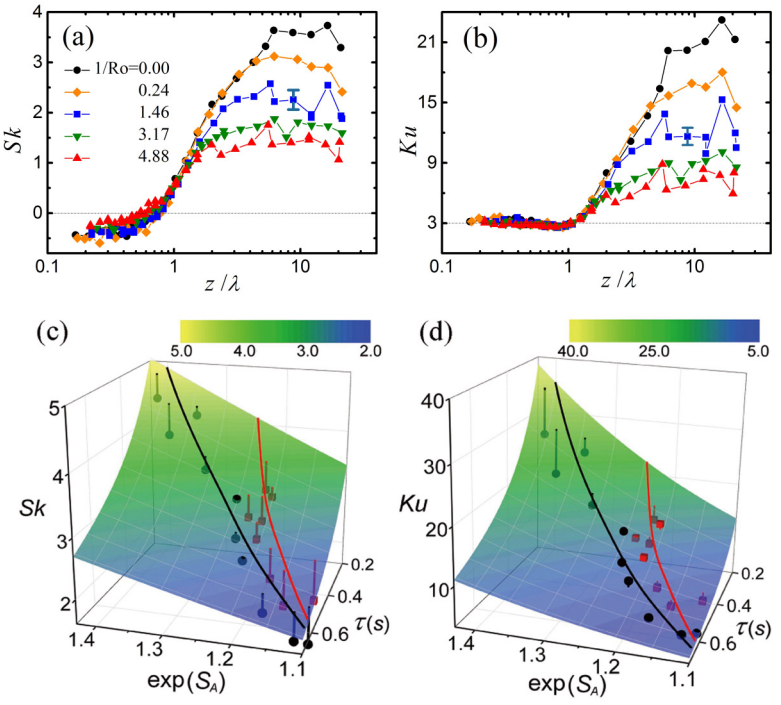

FIG. 3. Experimental results of (a) Sk(z) and (b) Ku(z) for Ra $= 4.22 \times 10^9$ and various Ro; representative error bars are included. Dashed lines show Sk $= 0$ and Ku $= 3$. Theoretical predictions of (c) Sk and (d) Ku as functions of $\exp(S_A)$ and τ are compared with the experimental data (closed circles). Values of Sk and Ku are presented by the coloration. Black circles denote $1/\mathrm{Ro} = 0.0$ and red circles $1/\mathrm{Ro} = 4.88$. The solid curves are spline fittings to the experimental data.

of the temperature time series between t_i and t_e [such as the red curve in Fig. 4(a)] are defined as the plume signals $\tilde{T}_p(t)$.

Based on this analysis, two dynamical characters of the plume signals are captured, that is, the plume temperature amplitude A and time width w. The plume time width is defined as the time interval between t_i and t_e, $w \equiv t_e - t_i$. We take the smaller value of $T(t_i)$ and $T(t_e)$ as the minimum plume temperature T_n and define the plume amplitude as $A \equiv T_m - T_n$. Figures 1(b) and 1(c) present the PDFs of the amplitude A and time width w for three values of Ro. Both A and w have log-normal distributions over the range of Ro studied. Log-normal distributions of these dynamical properties of thermal plumes have been previously observed in nonrotating RBC [34–36], which may arise from fragmentation processes as a consequence of the plume-bulk interaction [36]. It is remarkable that such a rule of distribution still dictates these plume properties under strong background rotations, in which the plume morphology and the turbulent bulk fluctuation may have been largely modified. It can be clearly seen in Figs. 1(b) and 1(c) that increasing the rotating rates enlarges the mean values of A and w, but reduces the half-width of the distributions of $P(A)$ and $P(w)$.

Rotations impact as well the shape of the temperature traces of thermal plumes. For a more quantitative description of the plume's temperature signal, we compose ensembles of plume signals. Figure 4(b) shows an example of the plume ensemble in which the peaks of each plume trace $T_p(t)$ are overlaid with the temperature and time span normalized by A and w individually, $T^* = (T - T_n)/A$ and $t^* = (t - t_m)/w$. The ensemble average of all temperature traces $G(t^*)$, shown by the black dotted line, typifies on average the shape of the thermal plumes measured at a certain fluid height and a rotating rate. We further characterize the function $G(t^*)$, extracting a set of plume-shape

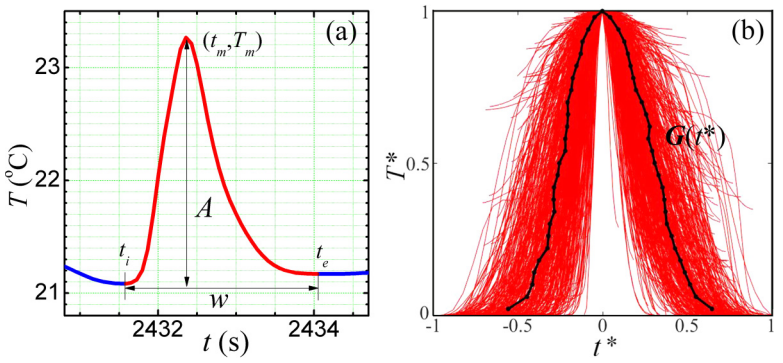

FIG. 4. (a) Example of the temperature signal captured from a thermal plume. The red curve is identified as the plume signal $\tilde{T}_p(t)$; the blue curves present the background fluid temperature. (b) Ensemble of temperature signals of thermal plumes (red curves). The black dotted line shows the ensemble average of the plume temperature $G(t^*)$. The temperature signals are taken with $\mathrm{Ra} = 4.22 \times 10^9$ and $1/\mathrm{Ro} = 1.46$ at a fluid height $z = 22\lambda$.

parameters $\alpha_1, \alpha_2, \ldots$, with the nth-order parameter defined as

$$\alpha_n = \int G^n(t^*)dt^*. \tag{1}$$

Here the integration is taken over the time span of $G(t^*)$. The plume-shape parameters appear to be weakly dependent on both the fluid height and the Rossby number. Results for α_2 are shown in Fig. 5(a).

C. Theoretical model for the statistics of temperature fluctuations

We have seen that despite the diversities in the temperature signals of thermal plumes shown Fig. 4(b), they possess similar dynamical properties from a statistical point of view. The temperature amplitude and time width of the plumes are both log-normally distributed. In addition, the temperature traces of the plumes are characterized by a common shape function $G(t^*)$ and the plume-shape parameters in Eq. (1). These observations suggest that simple theoretical expressions, in terms of the aforementioned general properties of the thermal plumes, are capable of describing the statistics of the temperature fluctuations. In the following, we derive a series of mathematical formulas to reveal the connections between the turbulent fluctuations in temperature and the dynamical properties of plumes and predict the statistical moments of the temperature fluctuations presented in Sec. III A.

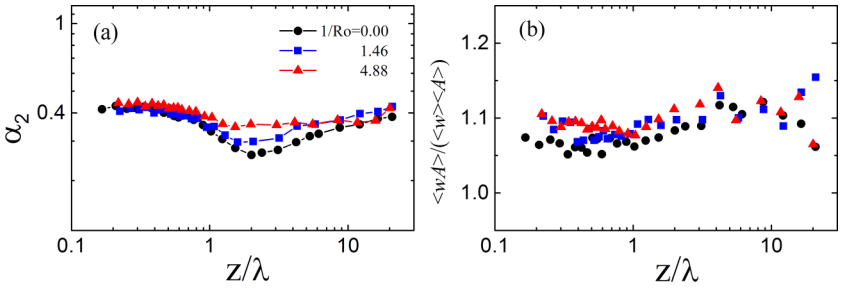

FIG. 5. Vertical profiles of (a) the plume-shape parameter α_2 and (b) the ratio between $\langle wA\rangle$ and $\langle w\rangle\langle A\rangle$ for $\mathrm{Ra} = 4.22 \times 10^9$ and various Rossby numbers.

Our experimental data reveal that the thermal fluctuations associated with the turbulent background are by far smaller than those associated with thermal plumes and that their contribution to high-order moments of temperature is negligible. We ignore their influence on the statistical properties of temperature fluctuations. In our theoretical treatment, we separate the temperature time series into two parts $T(t) = T_p(t) + T_b$, where the background temperature T_b is considered as a constant (i.e., the mean background temperature) and $T_p(t) = \tilde{T}_p(t) - T_b$ presents the relative plume temperature. After this approximation, we express the nth-order central moment of temperature as follows:

$$\langle (T - \langle T \rangle)^n \rangle = \langle (T_p - \langle T_p \rangle)^n \rangle = \sum_{l=0}^{n} (-1)^{n-l} C_n^l \langle T_p{}^l \rangle \langle T_p \rangle^{n-l}. \tag{2}$$

Here the binomial expansion is applied; C_n^l is the binomial coefficient. We consider a time series that consists of n_p plumes, and within the time span of the ith plume we sample m_i discrete temperature data points. The nth-order mean value of T_p is

$$\langle T_p^n \rangle = \frac{1}{N} \sum_{i=1}^{n_p} \sum_{j=1}^{m_i} (T_{ij})^n, \tag{3}$$

where T_{ij} is the temperature of the jth sampling point of the ith plume and N is the number of total sampling points. Since for a given Rossby number and a fluid height the shape of the plume signals can be approximated by their ensemble average $G(t^*)$, we determine the nth-order average of the ith plume, replacing in Eq. (3) the summation over j by integration in time:

$$\sum_{j=1}^{m_i} (T_{ij})^n = w_i A_i^n \sum_{j=1}^{m_i} (T_{ij}/A_i)^n / w_i = f w_i A_i^n \int_{(t_i - t_m)/w_i}^{(t_e - t_m)/w_i} G^n(t^*) dt^* = f w_i A_i^n \alpha_n. \tag{4}$$

We have applied in the last identity of Eq. (4) the definition of the plume-shape parameters α_n [Eq. (1)]. Since the mean temperature amplitude $\langle A \rangle$, the time width $\langle w \rangle$, and the plume-shape parameter α_n, which present the mean properties of the thermal plumes, are independent of the individual plume dynamics, we show in the following that the nth-order moment of temperature can be expressed simply in terms of these quantities. Based on Eqs. (3) and (4), the nth-order mean value of T_p is given by

$$\langle T_p^n \rangle = \frac{1}{N} \sum_{i=1}^{n_p} f w_i A_i^n \alpha_n = \frac{f \alpha_n}{N} \sum_{i=1}^{n_p} w_i A_i^n = n_p f \alpha_n \langle w A^n \rangle / N. \tag{5}$$

The plume-shape parameter α_n is the ensemble average of all plumes and is thus taken as a constant in the summation in Eq. (5). Our measurements further reveal that the plume amplitude A and time width w are independent, in the sense that the ratio of $\langle wA \rangle$ to $\langle w \rangle \langle A \rangle$ is close to unity (approximately equal to 1.1) and is nearly independent of the fluid depth or the Rossby number [Fig. 5(b)]. For this reason we assume that A and w are statistically uncorrelated and approximate that $\langle wA^n \rangle = \langle w \rangle \langle A^n \rangle$. Introducing the occupation time fraction of plumes $\tau = n_p f \langle w \rangle / N$, we simplify Eq. (5) as

$$\langle T_p^n \rangle = \alpha_n \tau \langle A^n \rangle. \tag{6}$$

Substituting Eq. (6) into Eq. (2) yields a general expression of any nth-order moment of temperature

$$\langle (T - \langle T \rangle)^n \rangle = \sum_{l=1}^{n} (-1)^{n-l} C_n^l \tau^{n-l+1} \alpha_l (\alpha_1)^{n-l} \langle A^l \rangle \langle A \rangle^{n-l} + (-\alpha_1 \tau \langle A \rangle)^n. \tag{7}$$

TABLE I. Fitting power exponents of four variables τ, $\langle A\rangle$, $\exp(S_A)$, and α_2 for $\mathrm{Ra} = 4.22 \times 10^9$ and various 1/Ro. Theoretical predictions of $\beta_{\mathrm{th}} = (2\beta_A + \beta_\tau + \beta_S + \beta_{\alpha_2})/2$ according to Eq. (9) are compared with the experimental results β_{expt}. The last two columns are the mean plume amplitude $\langle A\rangle$ and plume time width $\langle w\rangle$ measured at $z = 10\lambda$. The uncertainties in determining β are shown in parentheses.

1/Ro	β_A	β_τ	β_S	β_{α_2}	β_{th}	β_{expt}	$\langle A\rangle$	$\langle w\rangle$
0.00	0.49	0.51	−0.10	−0.13	0.63(±0.05)	0.57(±0.02)	1.47	1.42
0.49	0.41	0.28	−0.08	−0.16	0.43(±0.05)	0.38(±0.02)	1.67	2.02
1.46	0.34	0.24	−0.03	−0.15	0.37(±0.04)	0.31(±0.04)	1.72	2.50
2.20	0.24	0.26	−0.03	−0.10	0.31(±0.05)	0.29(±0.03)	1.69	2.67
3.17	0.21	0.28	−0.01	−0.10	0.30(±0.04)	0.24(±0.04)	1.92	3.02
4.88	0.15	0.30	−0.00	−0.05	0.20(±0.07)	0.24(±0.02)	2.19	3.23

As a consequence of Eq. (7), the temperature variance σ^2 can be derived as the second-order moment ($n = 2$)

$$\sigma^2 = \left(\tau\alpha_2\langle A^2\rangle - \tau^2\alpha_1^2\langle A\rangle^2\right). \tag{8}$$

Mathematically, since the PDFs of the temperature amplitude A follow a log-normal distribution, any nth-order mean of A can be expressed as

$$\langle A^n\rangle = \int_{-\infty}^{\infty} P(A)A^n dA = \langle A\rangle^n \exp\left(\frac{n(n-1)S_A}{2}\right). \tag{9}$$

Here $S_A \equiv \langle[\ln(A) - \langle\ln(A)\rangle]^2\rangle$ denotes the variance of $\ln(A)$, which reveals the fluctuating magnitude of the plume amplitude. Using Eq. (9), one can simplify the expression of the temperature variance

$$\sigma^2 = \tau\langle A\rangle^2\left[\alpha_2\exp(S_A) - \alpha_1^2\tau\right]. \tag{10}$$

Given by the profiles of τ, $\alpha_{1,2}$, A, and S_A, we present in Fig. 2(c) results of σ^2 for three rotating rates predicted by Eq. (10). One sees that the theoretical predictions agree with the experimental data. Evaluations of the various components in Eq. (10) suggest that the leading term dominates and σ^2 is mainly determined by $\tau\langle A\rangle^2\alpha_2\exp(S_A)$. Figures 2(d)–2(f) depict the statistical results of the vertical profiles of $\langle A\rangle$, τ, and $\exp(S_A)$. In the mixing zone these variables can be well described by power functions of the fluid height [hence $S_A(z)$ is a logarithmic function]. The second-order plume-shape parameter α_2, however, appears to be weakly dependent on z, as shown in Fig. 5(a). The best-fit exponents (β_A, β_τ, β_S, β_{α_2}) for several Ro are listed in Table I. Our prediction of the exponent of the temperature standard deviation $\beta_{\mathrm{th}} = (2\beta_A + \beta_\tau + \beta_S + \beta_{\alpha_2})/2$ is shown to be in good accord with the experimental data. Comparisons of the magnitudes of these exponents suggest that under the impact of rotation it is the increased mean plume amplitude $\langle A\rangle$ that mainly gives rise to a smaller decaying exponent β and stronger thermal fluctuations in the mixing zone. The increasing of the plume occupation time τ and the decreasing of S_A play a less important part in determining the rotation dependence of $\sigma(z)$.

Although the temperature variance outside the thermal BL is intensified under rotations, the magnitudes of higher-order moments (Sk and Ku) are substantially reduced [Figs. 3(a) and 3(b)]. The explanation of this opposite trend can be unified from our previous viewing of rotation-induced variations of the plume dynamics. Theoretical expressions for Sk and Ku can be obtained from Eq. (7):

$$\mathrm{Sk} = \frac{\tau\alpha_3\langle A^3\rangle - 3\tau^2\alpha_1\alpha_2\langle A^2\rangle\langle A\rangle + 2\alpha_1^3\tau^3\langle A\rangle^3}{\left(\tau\alpha_2\langle A^2\rangle - \tau^2\alpha_1^2\langle A\rangle^2\right)^{3/2}}, \tag{11}$$

$$\mathrm{Ku} = \frac{\tau\alpha_4\langle A^4\rangle - 4\tau^2\alpha_1\alpha_3\langle A^3\rangle\langle A\rangle + 6\alpha_1^2\alpha_2\tau^3\langle A\rangle^2\langle A^2\rangle - 3\alpha_1^4\tau^4\langle A\rangle^4}{\left(\tau\alpha_2\langle A^2\rangle - \tau^2\alpha_1^2\langle A\rangle^2\right)^2}. \tag{12}$$

Applying the rule of log-normal distributions of A [Eq. (9)] and keeping the leading-order terms in both the numerators and the denominators of Eqs. (11) and (12), respectively, one obtains the approximated relations

$$\mathrm{Sk} \approx \alpha_3 \alpha_2^{-3/2} \tau^{-1/2} \exp(3S_A/2), \tag{13}$$

$$\mathrm{Ku} \approx \alpha_4 \alpha_2^{-2} \tau^{-1} \exp(4S_A). \tag{14}$$

Note that Eqs. (13) and (14) are coarse expressions of Sk and Ku. Nonetheless, they provide hints to evaluate the main factors that lead to the declining of Sk and Ku under strong rotations. Since the plume-shape parameters α_n depend only weakly on the fluid height [see Fig. 5(a)], one sees that values of $\mathrm{Sk}(z)$ and $\mathrm{Ku}(z)$ are mainly given by the plume occupation time fraction τ and the variance S_A and are independent of the plume amplitude A. Using the measured profiles of $\tau(z)$ and $S_A(z)$, we depict in Figs. 3(c) and 3(d) our predictions of Sk and Ku as functions of τ and S_A given in Eqs. (13) and (14), which are compared to the experimental data. The values of Sk and Ku are both correlated to τ and S_A, for more ephemeral (smaller τ) and erratic (larger S_A) plume signals lead to a higher level of asymmetry of temperature distribution. Figures 3(c) and 3(d) further reveal that Sk and Ku are sensitively dependent on $S_A(z)$. The variance of the plume amplitude S_A, however, is significantly suppressed by the background rotations [Fig. 2(f)]. We suggest that this is the main reason responsible for the reduction of the high-order moments of the temperature fluctuation under strong rotations.

IV. CONCLUSION

Based on the present measurements and analysis, we infer that the prominent effects of rotation on thermal plumes are as follows. First, the rotational friction adjacent to the nonslip boundaries of the sample leads to the Ekman pumping process, in which the thermal plumes erupt more energetically from the BLs towards the interior fluid, resulting in greater plume amplitudes [Fig. 2(d)]. Our theoretical analysis suggests that this is the main factor that leads to the rotation-enhanced thermal fluctuations. Moreover, under strong rotations, as the thermal plumes are stretched into columnar vortical plumes, the mixing with the exterior flows through turbulent entrainment can be significantly reduced [37,38]. Thus the applied rotations provide a dynamical constraint to enhance the stability of the plume structure, as indicated by the observed suppression of the variance in the plume amplitude S_A [Fig. 2(f)]. This enables thermal plumes to impinge further into the fluid interior, with PDFs of temperature closer to a Gaussian distribution.

In summary, the present work combines high-precision measurements of the fluid temperature and in-depth analysis of the plume dynamics in turbulent rotating convection. We developed a theoretical approach of extracting the signals of coherent flow structures to reveal the physical origin of the statistical features of thermal fluctuations. We remark that the phenomenon that strong rotations reduce the turbulent mixing of coherent structures (including plumes, vortices, and density currents) with the ambient fluid and suppress their instabilities has been observed in laboratory experiments [39–41] and in field observations of oceanographic flows [42]. Although the various fluid systems are different in nature, the rotation-enhanced stability of the coherent flow structures may influence the turbulent thermal fluctuations in a variety of rotating flows through a similar principle proposed in this work. Challenges remain in future studies to further understand in general how fluctuations in turbulent flows are determined by coherent structures and extend the present investigation to broader parameter ranges relevant to natural flows in oceanographic and geophysical systems.

ACKNOWLEDGMENTS

We are grateful to R. Ecke and W. Ying for helpful discussions. This work was supported by the National Science Foundation of China through Grants No. 11572230, No. 11772235, and No. 1561161004.

[1] L. P. Kadanoff, Turbulent heat flow: Structures and scaling, Phys. Today **54**(8), 34 (2001).
[2] D. Lohse and K.-Q. Xia, Small-scale properties of turbulent Rayleigh-Bénard convection, Annu. Rev. Fluid Mech. **42**, 335 (2010).
[3] F. Heslot, B. Castaing, and A. Libchaber, Transition to turbulence in helium gas, Phys. Rev. A **36**, 5870 (1987).
[4] B. Castaing, G. Gunaratne, F. Heslot, L. Kadanoff, A. Libchaber, S. Thomae, X. Z. Wu, S. Zaleski, and G. Zanetti, Scaling of hard thermal turbulence in Rayleigh-Bénard convection, J. Fluid Mech. **204**, 1 (1989).
[5] T. H. Solomon and J. P. Gollub, Sheared Boundary Layers in Turbulent Rayleigh-Bénard Convection, Phys. Rev. Lett. **64**, 2382 (1990).
[6] E. D. Siggia, High Rayleigh number convection, Annu. Rev. Fluid Mech. **26**, 137 (1994).
[7] J. A. Glazier, T. Segawa, A. Naert, and M. Sano, Evidence against ultrahard thermal turbulence at very high Rayleigh numbers, Nature (London) **398**, 307 (1999).
[8] S. Q. Zhou and K.-Q. Xia, Scaling Properties of the Temperature Field in Convective Turbulence, Phys. Rev. Lett. **87**, 064501 (2001).
[9] A. Belmonte and A. Libchaber, Thermal signature of plumes in turbulent convection: The skewness of derivative, Phys. Rev. E **53**, 4893 (1996).
[10] S. Q. Zhou and K.-Q. Xia, Plume Statistics in Thermal Turbulence: Mixing of an Active Scalar, Phys. Rev. Lett. **89**, 184502 (2002).
[11] E. S. C. Ching, H. Guo, X. D. Shang, P. Tong, and K.-Q. Xia, Extraction of Plumes in Turbulent Thermal Convection, Phys. Rev. Lett. **93**, 124501 (2004).
[12] S. Grossmann and D. Lohse, Fluctuations in turbulent Rayleigh-Bénard convection: The role of plumes, Phys. Fluids **16**, 4462 (2004).
[13] G. Glatzmaier, R. Coe, L. Hongre, and P. Roberts, The role of the Earth's mantle in controlling the frequency of geomagnetic reversals, Nature (London) **401**, 885 (1999).
[14] M. S. Miesch, The coupling of solar convection and rotation, Solar Phys. **192**, 59 (2000).
[15] G. K. Vallis, *Atmospheric and Oceanic Fluid Dynamics* (Cambridge University Press, Cambridge, 2006), p. 745.
[16] J.-Q. Zhong, R. J. A. M. Stevens, H. J. H. Clercx, R. Verzicco, D. Lohse, and G. Ahlers, Prandtl-, Rayleigh-, and Rossby-Number Dependence of Heat Transport in Turbulent Rotating Rayleigh-Bénard Convection, Phys. Rev. Lett. **102**, 044502 (2009).
[17] R. J. A. M. Stevens, H. J. H. Clercx, and D. Lohse, Heat transport and flow structure in rotating Rayleigh-Bénard convection, Eur. J. Mech. B **40**, 41 (2013).
[18] Y. Liu and R. E. Ecke, Heat Transport Scaling in Turbulent Rayleigh-Bénard Convection: Effects of Rotation and Prandtl Number, Phys. Rev. Lett. **79**, 2257 (1997).
[19] R. P. J. Kunnen, H. J. H. Clercx, and B. J. Geurts, Heat flux intensification by vortical flow localization in rotating convection, Phys. Rev. E **74**, 056306 (2006).
[20] R. P. J. Kunnen, H. J. H. Clercx, and B. J. Geurts, Breakdown of large-scale circulation in turbulent rotating convection, Europhys. Lett. **84**, 2008 (2008).
[21] J. E. Hart, S. Kittelman, and D. R. Ohlsen, Mean flow precession and temperature probability density functions in turbulent rotating convection, Phys. Fluids **14**, 955 (2002).
[22] R. P. J. Kunnen, B. J. Geurts, and H. J. H. Clercx, Experimental and numerical investigation of turbulent convection in a rotating cylinder, J. Fluid Mech. **642**, 445 (2010).
[23] Y. Liu and R. E. Ecke, Local temperature measurements in turbulent rotating Rayleigh-Bénard convection, Phys. Rev. E **84**, 016311 (2011).
[24] J.-Q. Zhong, S. Sterl, and H.-M. Li, Dynamics of the large-scale circulation in turbulent Rayleigh-Bénard convection with modulated rotation, J. Fluid Mech. **778**, R4 (2015).
[25] S. Sterl, H.-M. Li, and J.-Q. Zhong, Dynamical and statistical phenomena of circulation and heat transfer in periodically forced rotating turbulent Rayleigh-Bénard convection, Phys. Rev. Fluids **1**, 084401 (2016).
[26] J.-Q. Zhong, H.-M. Li, and X.-Y. Wang, Enhanced azimuthal rotation of the large-scale flow through stochastic cessations in turbulent rotating convection with large Rossby numbers, Phys. Rev. Fluids **2**, 044602 (2017).

[27] A. Belmonte, A. Tilgner, and A. Libchaber, Temperature and velocity boundary layers in turbulent convection, Phys. Rev. E **50**, 269 (1994).
[28] C. Sun, Y.-H. Cheung, and K.-Q. Xia, Experimental studies of the viscous boundary layer properties in turbulent Rayleigh-Bénard convection, J. Fluid Mech. **605**, 79 (2008).
[29] Y. Wang, W. Xu, X. He, H. Yik, X. Ping, J. Schumacher, and P. Tong, Boundary layer fluctuations in turbulent Rayleigh-Bénard convection, J. Fluid Mech. **840**, 408 (2018).
[30] R. L. J. Fernandes and R. J. Adrian, Scaling of velocity and temperature fluctuations in turbulent thermal convection, Exp. Therm. Fluid Sci. **26**, 355 (2002).
[31] G. Ahlers, E. Bodenschatz, D. Funfschilling, S. Grossmann, X. He, D. Lohse, R. J. A. M. Stevens, and R. Verzicco, Logarithmic Temperature Profiles in Turbulent Rayleigh-Bénard Convection, Phys. Rev. Lett. **109**, 114501 (2012).
[32] Q. Zhou and K.-Q. Xia, Thermal boundary layer structure in turbulent Rayleigh-Bénard convection in a rectangular cell, J. Fluid Mech. **721**, 199 (2013).
[33] C. H. B. Priestley, Convection from a large horizontal surface, Aust. J. Phys. **7**, 176 (1954).
[34] S.-Q. Zhou, Y.-C. Xie, C. Sun, and K.-Q. Xia, Statistical characterization of thermal plumes in turbulent thermal convection, Phys. Rev. Fluids **1**, 054301 (2016).
[35] Q. Zhou, C. Sun, and K.-Q. Xia, Morphological Evolution of Thermal Plumes in Turbulent Rayleigh-Bénard Convection, Phys. Rev. Lett. **98**, 074501 (2007).
[36] J. Bosbach, S. Weiss, and G. Ahlers, Plume Fragmentation by Bulk Interactions in Turbulent Rayleigh-Bénard Convection, Phys. Rev. Lett. **108**, 054501 (2012).
[37] K. R. Helfrich, Thermals with background rotation and stratification, J. Fluid Mech. **259**, 265 (1994).
[38] K. Julien, S. Legg, J. Mcwilliams, and J. Werne, Plumes in rotating convection. Part 1. Ensemble statistics and dynamical balances, J. Fluid Mech. **391**, 151 (1999).
[39] H. J. S. Fernando and C. Y. Ching, Effects of background rotation on turbulent line plumes, J. Phys. Oceanogr. **23**, 2125 (1993).
[40] M. G. Wells, in *Particle-Laden Flow: From Geophysical to Kolmogorov Scales*, edited by B. J. Geurts, H. Clercx, and W. Uijttewaal (Springer, Berlin, 2007), Vol. 11, p. 331.
[41] C. Cenedese and C. Adduce, Mixing in a density-driven current flowing down a slope in a rotating fluid, J. Fluid Mech. **604**, 369 (2008).
[42] See, for instance, C. Cenedese and C. Adduce, A new parameterization for entrainment in overflows, J. Phys. Oceanogr. **40**, 1835 (2010) and references therein.